Friedel's salt profiles from thermogravimetric analysis and thermodynamic modelling of Portland cement-based mortars exposed to sodium chloride solution

Zhenguo Shi[a], Mette Rica Geiker[b], Barbara Lothenbach[c], Klaartje De Weerdt[b], Sergio Ferreiro Garzón[d], Kasper Enemark-Rasmussen[a,e], Jørgen Skibsted[a]*

[a.] Department of Chemistry and Interdisciplinary Nanoscience Center (iNANO), Aarhus University, 8000 C Aarhus, Denmark

[b.] Department of Structural Engineering, Norwegian University of Science and Technology (NTNU), 7491 Trondheim, Norway

[c.] Laboratory for Concrete & Construction Chemistry, Swiss Federal Laboratories for Materials Science and Technology (Empa), 8600 Dübendorf, Switzerland

[d.] Aalborg Portland A/S, Cementir Holding S.p.A., 9100 Aalborg, Denmark

[e.] Present address: Department of Chemistry, Technical University of Denmark, 2800 Kgs. Lyngby, Denmark

* Corresponding author. Department of Chemistry and Interdisciplinary Nanoscience Center (iNANO), Aarhus University, DK-8000 Aarhus C, Denmark. Tel: +45-87155946; Fax: +45 8619 6199. E-mail address: jskib@chem.au.dk (J. Skibsted).

Abstract

Thermogravimetric analysis (TGA), powder X-ray diffraction (XRD) and thermodynamic modelling have been used to obtain Friedel's salt profiles for saturated mortar cylinders exposed to a 2.8 M NaCl solution. Comparison of the measured Friedel's salt profiles with the total chloride profiles indicates that only a minor part of the chloride ions is bound in Friedel's in the studied Portland cement (P) and limestone blended (L) cement. The chloride binding capacity with respect to the formation of Friedel's salt by consumption of monocarbonate is reached for the P and L mortars, where only a fraction of about 20 % of the amount of C_3A is found to contribute to formation of Friedel's salt. Higher amounts of Friedel's salt are formed in the metakaolin containing mortars. However, the limited chloride ingress depths prevent quantification of the potential full chloride binding capacity of Friedel's salt in these mortars. The measured amounts of Friedel's salt by TGA and the portlandite profiles show that the maximum amount of Friedel's salt is found in the region with limited leaching of calcium, which is in good agreement with the predicted Friedel's salt profiles.

KEYWORDS

Friedel's salt profiles; thermogravimetric analysis; Portland cement-based mortars; chloride binding; total chloride profiles; thermodynamic modelling

1 Introduction

Reinforcement corrosion induced by chloride ions is one of the major mechanisms causing deterioration of reinforced concrete structures. When concrete is exposed to seawater or de-icing salts, chloride ions will penetrate into the concrete and if critical chloride levels are reached at the steel reinforcement, corrosion may occur. The resistance to chloride ingress for a given concrete is usually assessed by analyzing the total chloride profile, represented by the total chloride content as a function of the ingress depth [1-3]. The total chloride content refers to the sum of chloride ions which are chemically bound in Friedel's salt ($Ca_4Al_2(OH)_{12}$-$Cl_2 \cdot 4H_2O$), chloride ions which are physically adsorbed in the diffuse layer of the calcium-silicate-hydrate (C-S-H) phase, as well as free chloride ions present in the pore solution. The former two types of chloride ions are often both referred to as bound chlorides.

There are conflicting reports on the contribution of the chemically bound, physically adsorbed and free chloride ions to the total chloride content. Loser *et al.* [4] found that only a small fraction of the chloride ions is bound by cement hydrates and that the largest fraction of chloride is present in the pore solution. Several review articles [5-7] have addressed that the main chloride binding originates from the tricalcium aluminate ($Ca_3Al_2O_6$: C_3A) or ferrite ($Ca_2Al_{1-x}Fe_xO_5$: C_4AF) phases through formation of Friedel's salt and its iron-containing analogue. On the other hand, Tang and Nilsson [8] suggest that the major binding is attributed to physical adsorption on the C-S-H. However, the adsorption of chlorides on the C-S-H varies with the Ca/Si ratio of the C-S-H and the pH value of the exposure solution [9-12]. Experimental and modelling results [13] suggest that the chloride ions associated with the C-S-H are mainly present in the diffuse layer of the C-S-H surface, which is positively charged in the presence of high calcium concentrations. The impact of chemical binding and physical adsorption of chlorides on chloride ingress is also disputed. Some studies [7, 14, 15] stated that the interactions of chloride with cement hydrates may retard the chloride transport and change the shape of the chloride profiles. However, Loser *et al.* [4] concluded that the impact of chloride binding on chloride ingress is less important compared to the physical restraint of the pore structure. Moreover, a recent study [16] reported that physical adsorbed chloride ions pass easily through the diffuse layer of the C-S-H and thereby do not limit the ingress of chloride.

These contradictory statements found in the literature underline the importance of valid and reliable experimental methods to quantify the chlorides in the different states, *i.e.*, as free, chemically bound or physically adsorbed chloride ions. This paper focuses on the quantification of the amount of chemically bound chloride, *i.e.*, chloride ions bound in Friedel's salt.

Quantification of Friedel's salt by XRD is possible for paste samples. This method is also applicable for mortar samples but the accuracy is significantly reduced by the presence of a large amount of quartz from the sand aggregate. Alternatively, TGA may be used, as the presence of sand only dilutes the sample but does not lead to additional thermal events. TGA has been used to identify Friedel's salt in cement pastes or mortars in several studies [12, 17, 18]. However, only one study [18] used TGA for the quantification of Friedel's salt in Portland cement-based pastes and the methodology used for the quantification was not described.

The first derivative of the TG curve (DTG) for synthesized Friedel's salt is shown in Fig. 1, as reported in three earlier studies [19-21]. The thermal decomposition of Friedel's salt results in two major DTG peaks in the temperature ranges of 30 ~ 180 °C and 180 ~ 450 °C. It should be noted that two well-defined single peaks were observed in two previous studies [19, 20], rather than a splitting of the second peak (180 ~ 450 °C) as observed by Lothenbach *et al*. [21]. The reason for this discrepancy is not clear. Nonetheless, the weight losses associated with the lower and higher temperature intervals have the same ratio of 4:6 in the three different studies. The fixed ratio between the two weight losses is ascribed to the layered structure and composition of Friedel's salt with positively charged main layers, $[Ca_4Al_2(OH)_{12}]^{2+}$, comprising 12 hydroxyl groups and negatively charged interlayers [$2Cl^-$, $4H_2O$] containing four water molecules [19]. Friedel's salt in cement pastes or mortars is usually identified by the second DTG peak [12, 17].

The aim of this work is to evaluate of the contribution of Friedel's salt to the chloride binding in Portland cement – calcined clay – limestone mortars exposed to a NaCl solution by employing the TGA method and thermodynamic modelling. The measured and calculated Friedel's salt profiles are compared for evaluation of the contribution of Friedel's salt to the chloride binding for mortars under chloride ingress.

2 Experimental

The total chloride profiles were measured on mortar samples which were cast, cured and analyzed according to procedures reported recently [22] and also described in this work. A white Portland cement is used for the mortars, since the hydration of identical paste blends have been studied in detail, including determination of the hydration kinetics for the principal phases and the formed hydrates by ^{29}Si MAS NMR and powder XRD [23]. These data are partly used in the thermodynamic modelling of the phase assemblages of the mortars in the present work.

2.1 Materials

The binders used in this study were made from a white Portland cement (wPc, CEM I 52.5 N) and three supplementary cementitious materials (SCMs): metakaolin (MK), white silica fume (SF) and limestone (LS). The wPc was produced by Aalborg Portland A/S, Denmark, and included 3.1 wt.% LS, 4.1 wt.% gypsum and 1.9 % wt.% free lime. The MK was produced in the laboratory from kaolinite (Kaolinite Supreme^{TM} from Imerys Performance Minerals, UK) by thermal treatment at 550 ^{o}C for 20 h and its actual Si/Al ratio of 1.13 accounts for a 2 wt.% quartz impurity in the material. The densified SF was purchased from Elkem A/S, Norway. The LS was a Maastrichtian chalk from Rørdal, Northern Denmark. The chemical compositions of the starting materials determined by X-ray fluorescence (XRF) are given in Table 1. The wPc contained 64.9 wt.% alite ($3CaO{\cdot}SiO_2$: C_3S) and 16.9 wt.% belite ($2CaO{\cdot}SiO_2$: C_2S) and 7.8 wt.% calcium aluminate ($3CaO{\cdot}Al_2O_3$: C_3A), where the content of the silicate phases was determined by ^{29}Si MAS NMR and the quantity of C_3A by mass balance calculations [24]. The small amount of iron in the wPc, determined by XRF analysis, is expected to be incorporated as guest ions in the C_3S, C_2S and C_3A phases. The determined mineral composition has taken into account the quantities of aluminum guest ions in C_3S and C_2S, employing the atomic ratios between Al and Si in C_3S and C_2S given by Taylor [25]. The sand used for the mortars was a CEN reference sand (Normensand GmbH, Germany), which has a silica content of at least 98 wt.% and a density of 2650 kg/m^3. A polycarboxylic ether (PCE) based superplasticizer (SP, Glenium 27, BASF) was used to achieve similar flow for all mortars.

2.2 Mortar preparations

The compositions of the binders (Table 2) targeted a replacement of 35 wt.% of the white Portland clinkers by SCMs which is the maximum replacement for CEM II/B cements with reference to the EN 197-1 standard. The small amount of LS (3.1 wt.%) in the wPc resulted in actual binder compositions with 31.9 wt.% replacement of the wPc. The P mortar, produced by pure wPc, and the L mortar, containing a combination of 68.1 wt.% wPc and 31.9 wt.% LS, were prepared as reference mortars. The ML and M mortars were produced by partially replacing wPc with MK (1:1 clay) and/or LS. The MS and MSL mortars were produced by partially replacing wPc with MK, SF and/or LS, where the ratio between MK and SF was fixed to mimic a 2:1 clay. However, the actual Si/Al ratio of 2.36 for the MS and MSL blends is higher than the ideal 2:1 ratio in order to account for the partial substitution of Al in the octahedral layers, for example the Al by Mg substitution found in montmorillonite [26]. The

evolution in compressive strength with hydration time has been investigated for similar mortars in a parallel study [27] which revealed synergetic effects between MK and LS as well as MS, SF and LS, where the highest compressive strengths were observed for the mortars with MK/(MK+LS) = 0.75 and (MK+SF)/ (MK+SF+LS) = 0.75, respectively.

The binders were used to produce mortars with a constant water-to-binder ratio (w/b = 0.5) and binder-to-sand ratio (b/s = 1/3), both ratios by weight. The dosage of superplasticizer was SP/(MK+SF) = 0.04 for the mortars including SF, whereas it was adjusted to SP/MK = 0.07 for the mortars without SF to achieve a flow within ± 5% of the flow of the reference P mortar. The cement blends, sand and water were mixed and cast into polypropylene bottles (ø50 mm, 125 ml). A small amount of water was added on top of the mortar to keep the mortar saturated and to compensate for self-desiccation caused by early-age chemical shrinkage [28]. Mortars were demolded after 24 hours and cured in demineralized water for 91 days in an airtight bucket with a water/mortar ratio of 3:1 by volume at 20 ± 1 ºC. At the last week of curing, the mortar cylinders were treated by removing (wet cutting) about 5 mm mortar from both ends in order to remove the paste-rich layer, which potentially has carbonated and leached. Immediately after cutting, the mortars were placed on a table and exposed to the natural environment in the laboratory for 2 hours to surface dry. Subsequently, a two-layer epoxy coating (about 1 mm thickness) was applied on the bottom and circumference surfaces, leaving only the top surface uncoated for exposure. When the epoxy had hardened, the uncoated surfaces of the mortars were submerged in a small amount of demineralized water for re-saturation until the end of the 91 days of curing.

2.3 Total chloride profile analysis

The total chloride profiles were analyzed according to the procedure described recently in ref. [22]. After 91 days of curing, three epoxy-coated mortar cylinders from each blend were exposed to 700 ml 2.8 M NaCl solution in an airtight box for 35 days at 20 ºC. The solutions were replaced weekly in order to maintain an approximate constant chloride concentration in the exposure solution. At the end of exposure, one of the three mortar cylinders from each box was split along the chloride ingress direction. The chloride penetration depth was measured by spraying 0.1 M $AgNO_3$ solution on the fresh split surface of one half-cylinder. The remaining two full mortar cylinders and the one half-cylinder were profile ground with a layer thickness increasing from 1 to 4 mm. The total depth of grinding was determined based on the chloride penetration depth measured by the $AgNO_3$ solution. The powder samples from each layer were collected for total chloride profile analysis. The powders were firstly dried in an oven at 105 ºC

for 24 hours. The moisture content was calculated according to the mass loss after drying. The dried powders were dissolved in 1:10 HNO_3 solution at 80 °C. The volume of solution used to dissolve the paste was 20 ml for 2 g powder (from and close to outer layer) and 40 ml for 4 g powder (from inner layers). The powder-acid suspension was stirred and left to rest for 2 hours. The resulting solutions were subsequently filtrated, and 15 ml filtrate was sampled. For samples from and close to the outer layer, 1.0 ml filtrate was titrated with a Titrando 905 titrator (Metrohm) using a 0.010 M $AgNO_3$ solution. For filtrates with low chloride concentrations, *i.e.*, for samples from inner layers, 10 ml of filtrate was titrated and 1.0 ml of acetic acid (EMSURE®) was added to the filtrate to improve detection. The total chloride content was reported as mass percentage of dried mortars at 105 °C.

2.4 Assessment of Friedel's salt and portlandite content by TGA

Thermogravimetric analysis (TGA) was performed on the powdered mortar samples. A Mettler Toledo TGA/SDTA 851 instrument was used. About 50 mg of the powdered sample was loaded in a 150 µm alumina crucible. The weight loss of the samples was monitored while heating from 30 °C to 980 °C at a rate of 20 °C/min and purging with 50 ml/min N_2. The weight loss and quantified data were reported as mass percentage of dried mortars at 500 °C.

According to the 4:6 ratio in Friedel's salt between interlayer water and main layer water, confirmed for the synthesized samples as mentioned in the introduction, the quantity of Friedel's salt in mortars can be assessed by determination of the content of the main layer water (~230 – 410 °C). Fig. 2 shows the first derivatives of the TGA curves (DTG) for a powdered mortar sample obtained at 1~2 mm chloride penetration depth, a powder sample from the region without ingress of chloride ions (*e.g.* 8~12 mm), and for synthesized Friedel's salt. The temperature range between the weight loss of C-S-H, ettringite, monocarbonate and strätlingite at temperatures up to 230°C on one hand and the weight loss of portlandite above 410 °C on the other hand, limits the interval where the weight loss due to the decomposition of the main layer water for Friedel's salt can be observed, as apparent from Fig. 2. The quantification was performed by the construction of a baseline on the DTG curve for the chloride-containing sample based on the baseline for the reference sample, which does not include chloride. The area marked on the DTG curve for the chloride-containing sample was then integrated, m_{H}, and the content of Friedel's salt in the mortar was calculated according to the equation:

$$m_{FS} = \frac{M_{FS}}{6 \times M_H} m_H = \frac{561.3}{6 \times 18.02} m_H \quad (1)$$

Here, m_{Fs} is the mass fraction of Friedel's salt in the mortar (wt.%), m_{H} is measured loss of water by TGA from the main layer (wt. %), M_{Fs} is the molar mass for Friedel's salt (561.3 g/mol) with the chemical composition $Ca_4Al_2(OH)_{12}Cl_2{\cdot}4H_2O$, and M_{H} is the molar mass of H_2O (18.02 g/mol). The portlandite content was quantified by determination of the weight loss in the temperature range from ~400 – 500 °C by integrating the area below the baseline (tangential method) and this value was scaled according to the equation:

$$m_{CH} = \frac{M_{CH}}{M_H} \times m = \frac{74.09}{18.02} \times m \quad (2)$$

where m_{CH} is the mass fraction of portlandite in the mortar (wt.%), m is the loss of water from portlandite (wt.%), M_{CH} is the molar mass (74.09 g/mol) of portlandite in the form of $Ca(OH)_2$ and M_{H} is the molar mass (18.02 g/mol) of H_2O.

2.5 X-ray diffraction analysis

The powder X-ray diffraction (XRD) analysis was carried out with a CubiX3 diffractometer (PANalytical, NL) between Bragg angles (2Θ) of 5° and 65° using a step size of 0.02°. The powdered mortar samples used for both the total chloride profile analysis and the TGA measurements were prepared by mixing and grinding 1.80 g of sample and 0.20 g of high-purity anatase (TiO_2) in a planetary ball-mill for 45 seconds at 350 rpm. The mixed powder was then lightly pressed into a pellet with a smooth surface. The acquired diffractograms were analyzed by the Rietveld procedure, using starting parameters for the individual phases obtained from the Inorganic Crystal Structure Database (ICSD). Only the scale factor, unit cell dimensions and profile parameters were refined in the Rietveld refinement process. The addition of an internal standard (anatase) allowed for a possible quantification of the observed phases (*e.g.* Friedel's salt and portlandite), despite the presence of amorphous phases and a large amount of quartz in the powdered mortar samples.

2.6 Thermodynamic modelling

Thermodynamic modelling can be used to calculate the potential of chloride binding in Friedel's salt for different cement blends. This was carried out by using the Gibbs free energy minimization program, GEMS 3.3 [29, 30], which calculates the equilibrium phase assemblages in chemical systems from their total bulk elemental composition. The default databases were expanded with the CEMDATA14 database [31-33]. The data include solubility products of the solids relevant for cementitious systems and for Friedel's salt. In the present

calculations, the influence of physical adsorption of chloride on the C-S-H phase has been neglected as adequate thermodynamic models are not yet available. The uptake of aluminum (Al) and sulfur (S) by the C-S-H phase is taken into account using the reported Al/Si [23] and S/Si [34] ratios for C-S-H formed in similar systems and synthetic C-S-H phases with different Ca/Si ratios, respectively, as summarized in Table 2. The calculation of the reaction is restricted with the degree of hydration for the same binder blends reported in [23]. The release of Al from C_3S and C_2S during hydration is also considered. The changes in phase assemblages upon exposure to a NaCl solution were predicted for the different blends. The NaCl concentration (2.8 M) used in the calculations was identical to the chloride ingress experiments. The activity coefficients were calculated using the extended Debye–Hückel equation in the Truesdell–Jones form with the ion size and the extended-term parameter for NaCl ($\mathring{a}$ = 3.72 Å and b_γ = 0.064 kg/mol) [35], which is applicable up to an ionic strength of approx. 1 - 2 M [36]. While at this high ionic strength the use of the Pitzer activity corrections would result in more precise aqueous concentrations, the use of extended Debye–Hückel equation has no significant effect on the amount of solid phases calculated in the system studied. The quantity of NaCl solution in the calculations was varied from 0 to 100,000 ml NaCl solution (2.8 M = 163.7 g/l) per 100 g anhydrous cement. The results are presented in g per 100 g anhydrous cements as a function of the volume of the added solution. This approach allows prediction of the progressive change in phases, and thus it can be used to mimic the ingress of chloride ions, assuming that the surface of the mortar is in contact with an infinite amount of Cl^- ions in solution and that the center of the mortar does not contain chloride ions.

3 Results

3.1 Total chloride profiles

The total chloride profiles for all mortars hydrated for 91 days and then exposed to 2.8 M NaCl solution for 35 days are shown in Fig. 3. The results show that the total chloride content decreases with increasing chloride penetration depths for all tested blends. The L mortar exhibits the deepest chloride penetration depth and the highest total chloride content at any depth excluding the outer layer, whereas the MK mortars show the lowest chloride penetration depths. The total chloride profiles are similar for the different MK-containing mortars. Pore structure data, and in particular the threshold pore size obtained by mercury intrusion porosimetry (MIP), have been obtained for the different blends in related studies from our group [37, 38]. Key data from that work are summarized in Table 3 which allows comparison

of the pore structure data with the apparent chloride diffusion coefficient, D_e, obtained by fitting the total chloride profiles with the error function solution to Fick's second law. A lower diffusion coefficient is observed for the blends with a lower threshold pore radius (Table 3) where it should be noted that a limited number of data points are available for the determination of the diffusion coefficient. Thus, the highest and lowest chloride ingress resistance, observed for the MK and L mortars, may be related to the lowest and highest pore diameters observed by MIP, respectively, and the resulting differences in pore connectivity for the MK and L mortars.

3.2 Measured phase changes and Friedel's salt / portlandite profiles from TGA

The DTG curves for the powdered samples taken at different chloride ingress depths of the mortars after chloride exposure for 35 days are shown in Fig. 4. Three major weight losses are observed for the samples obtained from the inner core of the mortars which do not contain chloride, *i.e.*, C-S-H/AFm/AFt phases (30 ~ 230 °C), portlandite (410 ~ 520 °C) and $CaCO_3$ (520 ~ 760 °C). The DTG peak related to the decomposition of monocarbonate (at ~150 °C) is much clearer observed for the MK mortar samples than for the P and L mortar samples which reflects that more alumina is present due to the reaction of MK. In addition, a small shoulder associated with the decomposition of strätlingite (at ~220 °C) is observed for the M and MS mortars. The identified phases are consistent with those observed by XRD, ^{29}Si MAS NMR and predicted by thermodynamic modelling on the same paste samples [23]. Close to the exposed surface of the mortars, where the samples are in contact with the NaCl solution, an additional weight loss (230 ~ 410 °C) is observed which is associated with the release of the six main layer water molecules of Friedel's salt. Moreover, the occurrence of another peak at lower temperature (below 150 °C) associated with the release of the four interlayer water molecules of Friedel's salt is also identified. The data in Fig. 4 reveals that the formation of Friedel's salt is accompanied by the decomposition of monocarbonate for all mortars, and also of strätlingite for the M and MS mortars. In addition to the observation of the transformation from AFm phases (monocarbonate and strätlingite) to Friedel's salt, leaching of portlandite and even the destabilization of limestone by the NaCl solution are observed at the surface of the mortars.

Based on the data presented in Fig. 4, the changes in the amounts of Friedel's salt and portlandite can be assessed using the method described in section 2.4. The obtained Friedel's salt and portlandite profiles are shown in Fig. 5 and Fig. 6. The results show that the formation of Friedel's salts is observed at deeper depths for the P and L mortars than for the MK-

containing mortars. Near to the surface, higher amounts of Friedel's salt are observed in the MK mortars (except for the M mortar) than in the P and L mortars as a result of the availability of additional aluminum, which is in accordance with previous studies of alumina-rich SCM's [7, 39, 40]. Overall, the amounts of Friedel's salt decrease with increasing depth with exception of the outermost layer, where a significant reduced amount of Friedel's salt is observed (except for the ML and M mortars). The reduction in the quantity of Friedel's salt is expected to be caused by a severe leaching of calcium ions at the 0 – 1 mm depth. Interestingly, the maximum amount of Friedel's salt is formed where limited calcium leaching (1 – 2 mm) has occurred as shown in Fig. 6. This is further supported by thermodynamic modelling (*section 3.4*). A reduction in the chloride content at the exposure surface has also been reported in other studies [3, 41-44]. Moreover, it should be noted that the changes in $CaCO_3$ content, obtained from Fig. 4, are so small that they do not justify a reduction in portlandite by carbonation. As a result of the very limited chloride penetration depth for the MK mortars, the diffusion zone and the leaching zone overlap. In summary, the phase assemblage of the samples at the outermost layer is different from the subsequent inner layers as reflected by the reduction of total chloride (Fig. 3), calcite (Fig. 4), Friedel's salt (Fig. 5), and portlandite (Fig. 6) in the outer layer. This will lead to an underestimation of the chloride binding capacity of the MK mortars, which is expected to be higher as a result of the larger fraction of alumina in these mortars.

3.3 X-ray diffraction analysis

The diffraction patterns for the samples taken from 1 – 2 mm depths of the P, M, MS and MSL mortars are shown in Fig. 7. The recorded diffractograms are dominated by the quartz reflection due to the presence of the sand aggregate in the mortars. Reflections of Friedel's salt and portlandite are observed at 11.4° and 18.3° 2θ, respectively [45]. The quantities of both phases have been determined by Rietveld analysis of the XRD patterns for the P, L, MS, and MSL mortars and the results are summarized in Table 4. It should be noted that the high quantity of sand in the samples prevent an accurate analysis of the recorded diffractograms. Thus, the results should be considered as estimates only. However, it can be seen from the data in Table 4 that there is a general agreement between XRD and TGA for the amounts of Friedel's salt and portlandite.

3.4 Predicted phase assemblages and Friedel's salt profiles

The phase assemblages of the hydrated paste samples have been predicted by thermodynamic modelling (Fig. 8, right-hand side of each graph), employing the measured degrees of hydration for the principal phases (alite, belite, and metakaolin) in the paste samples, as

determined by ^{29}Si MAS NMR analyses of the samples after 91 days of hydration in [23]. For the P paste, the major hydrate phases prior to chloride ingress are C-S-H, ettringite, portlandite, and a small quantity of monocarbonate. The modeled data for the L paste is not included here, since the same phases are predicted as for the P paste, however, with an increased amount of calcite and smaller quantities of the other hydrates. For the ML and M samples, portlandite is predicted to be absent as a result of the pozzolanic reaction of metakaolin. Strätlingite and monocarbonate are predicted for the M and ML pastes where the quantity of monocarbonate is lower for the M paste due to the limited availability of limestone. Modelling for the MSL and ML samples (not shown) show the same phases as predicted for the ML and M pastes, respectively. The phase assemblages calculated by thermodynamic modelling are in good agreement with experimental observations by XRD and ^{29}Si MAS NMR for hydrated paste samples of blends with the same compositions [24].

The changes in the phase assemblages caused by chloride ingress are predicted by thermodynamic modelling by stepwise adding increased amounts of the 2.8 M NaCl solution to the system, as described in section 2.6. It should be noticed that the exposure to equimolar Na^+ and Cl^- concentrations is a simplification as Na^+ and Cl^- ions do not diffuse into concrete in an equal manner [3, 43, 44]. Upon the ingress of the NaCl solution (from left to right in the graphs of Fig. 8), thermodynamic modelling predicts the destabilization of monocarbonate and the formation of Friedel's salt and calcite for the P, L, ML and MSL blends. Strätlingite is predicted to decompose for the M and MS samples before monocarbonate, resulting in the formation of more Friedel's salt. The TGA data for the powders sampled at different depths of the mortars confirm the transformation of strätlingite and monocarbonate into Friedel's salt, as predicted by thermodynamic modelling. With increasing amounts of the NaCl solution, thermodynamic modelling predicts that also portlandite and ettringite are destabilized due to the leaching of calcium while somewhat more Friedel's salt is formed. At the surface of the mortars (heavily leached area), which experiences the highest amount of the NaCl solution, even Friedel's salt and the C-S-H phase become unstable due to leaching. The destabilization of portlandite is confirmed by the TGA measurements for the outermost 2 mm layers of the mortars (Fig. 4 and Fig. 6). However, the complete destabilization of ettringite and C-S-H, as predicted at the surface by thermodynamic modelling, is not observed in Fig. 4. This could be a result of the limited depth of the leached zone (< 100 µm as observed in refs. [42, 43]) compared to the sampling size (0 ~ 1 mm) as well as the short exposure time.

Fig. 9 shows the calculated amounts of chloride bound in Friedel's salt (left-hand scale) and the Friedel's salt profiles (right-hand scale) for the studied samples. Generally, similar trends

are observed for the measured (TGA, Fig. 5) and predicted (Fig. 9) Friedel's salt profiles, *i.e.*, a small amount of Friedel's salt for low amounts of the NaCl solution and a higher binding capacity for the mortars with metakaolin. In addition, thermodynamic modelling predicts two different leaching zones which can be defined as "limited leaching" and "advanced leaching" zones, corresponding to the decomposition of ettringite and a further decomposition of Friedel's salt, respectively. The two leaching zones are also seen from the experimental data, as shown in Fig. 5 and Fig. 6, where the zones are identified by comparing the changes in the measured amounts of Friedel's salt and portlandite with those predicted by thermodynamic modelling. The results in Fig. 5 and Fig. 9 show an increased contribution in chloride binding by Friedel's salt formation in the limited leaching zone, and reduced formation of Friedel's salt in the advanced leaching zone. The predicted chloride binding capacity with respect to formation of Friedel's salt by consumption of monocarbonate for the P and L mortars (at 13 ml NaCl solution / 100 g anhydrous cements in Fig. 9) is found to be similar to the measured chloride binding. Note that thermodynamic modelling predicts a higher maximum chloride binding than the measured maximum chloride binding, especially for the MK containing mortars. This reflects that the sampling width for the TGA and XRD measurement is approx. 2 mm and thus, the measured data should be considered as average values over the profile rather than maximum values, as predicted by thermodynamic modelling in the present study and measured by SEM-EDS analysis in recent studies [43, 44].

4 Discussion

In order to evaluate the relation between the amount of Friedel's salt and the total content of chloride, the amount of chloride in Friedel's salt is plotted as a function of the total chloride content for the P and L mortars in Fig. 10. The results indicate that the amount of Friedel's salt is nearly constant with a minor increase with increasing total chloride content in the range with leaching from 0.6 g to 1.1 g total Cl per 100 g dry mortar. This corresponds to depths of 2 – 5 mm and 2 –10 mm for the P and L mortars, respectively (Fig. 5), and it suggests that the maximum chloride binding capacity by Friedel's salt formation caused by the depletion of monocarbonate is reached. The minor increased amount of Friedel's salt in this interval is ascribed to the decomposition of ettringite according to thermodynamic modelling, where the predicted Friedel's salt profiles in Fig. 9 confirm this trend. The phase assemblages in Fig. 8 show that the apparent plateau in the Friedel's salt content as a function of the total chloride content (Fig. 10) is caused by the complete transformation of monocarbonate into Friedel's salt prior to the complete destabilization of ettringite. Such trends are not observed for the MK

mortars, neither from experiments (Fig. 5) nor from calculations (Fig. 9). Although the amount of C_3A in the L blend is lowered through the dilution of the cement by the 31.9 wt.% limestone in the L mortar as compared to P mortar, comparison of the curves for P and L mortars in Fig. 10 reveals that the Friedel's salt content is reduced to a lower extent than expected from a dilution of the cement by 31.9 wt%. This indicates that a higher fraction of Friedel's salt is formed per unit of C_3A content for the L mortar. This observation is supported by thermodynamic modelling where the calculated Friedel's salt profiles in Fig. 9 show that the amount of Friedel's salt formed prior to decomposition of ettringite in the L mortar is similar to that formed in the P mortar. The prediction of a higher amount of Friedel's salt than expected for the L mortar, can partially be attributed to the release of a relatively higher fraction of Al guest ions from alite and belite as a result of their higher degrees of hydration as compared to those for observed for these phases in the P mortar, as reported from ^{29}Si NMR studies of similar paste samples [23].

The contribution of Friedel's salt to chloride binding can be evaluated by comparison of the bound chloride in Friedel's salt with the total chloride profiles as shown in Fig. 11 for the P, L, and MK-containing mortars. It is found that the chloride from Friedel's salt is about 0.1 wt.% for the P and L mortars, which is 10 times less than the maximum total chloride content (about 1.0 wt% of mortar) excluding the experimental data for the surface layer. The difference between total chloride content and the amount of chloride bound in Friedel's salt originates from chloride ions present in the pore solution and in the diffuse layer of the C-S-H phase [16]. For the MK mortars, the bound chloride in Friedel's salt range from 0.1 to 0.2 wt.% of the dry mortar, however, the data exhibit a rather large uncertainty due to the limited chloride ingress depth studied. Considering the total C_3A content (7.8 wt.%) determined for the white Portland cement, it can be calculated that only a fraction of about 20 % of the C_3A has been converted into Friedel's salt for the P mortar as measured by TGA. This is in good agreement with the thermodynamic calculations, where only 20 % of the hydrated C_3A phase leads to formation of monocarbonate. Thermodynamic modelling predicts that a larger fraction of ettringite transforms into Friedel's salt near the surface, which is not clearly observed from the experimental data in this work. The maximum measured chloride binding observed in the present study corresponds to the complete conversion of monocarbonate into Friedel's salt for the P and L mortars. Elakneswaran *et al*. [46] have studied chloride binding of hydrated cement paste using a Portland cement with a higher aluminate and ferrite content (C_3A = 9.7 wt.% and C_4AF = 8.8 wt.%) compared to the cement used in the present work. They found that the total amount of bound chloride (measured by the equilibrium concentration technique) and the

amount of chloride bound in Friedel's salt (by XRD Rietveld analysis) are 1.3 wt.% and 0.6 wt.%, respectively, for samples exposed to a 1.0 M NaCl solution. This is about twice as much as measured in this study which probably relates to the difference in the aluminate and ferrite contents of the cements.

5 Conclusion

Thermogravimetric analysis (TGA), powder X-ray diffraction (XRD) and thermodynamic modelling have been employed to assess the chloride binding in Friedel's salt for Portland cement-based mortars upon chloride ingress. The transformation of monocarbonate and/or strätlingite into Friedel's salt is observed by TGA and XRD and predicted by thermodynamic calculations. The amounts of Friedel's salt measured by TGA are comparable to the amounts obtained by XRD-Rietveld and thermodynamic calculations for both the Portland (P) and limestone blended (L) mortars. Thus, the results indicate that TGA may be an efficient and valuable tool to estimate the amount of Friedel's salt in Portland cement blends exposed to a chloride environment. However, reference samples that have not been exposed to chloride should always be analysed at the same time to secure that no other phases interfere the TGA quantification of Friedel's salt.

Comparison of the Friedel's salt profiles measured by TGA with the total chloride profiles shows a relatively low contribution of Friedel's salt to the measured total chloride content. For the P and L mortars, the TGA data together with the chemical composition of the white Portland cement indicates that only a fraction of about 20 % of the C_3A content contributes to the formation of monocarbonate which later transforms into Friedel's salt. Thus, depending on the alumina content, the contribution from Friedel's salt formation on chloride binding in Portland cement and Portland cement – limestone blends may be much less than stated in some earlier studies in the literature.

The maximum chloride binding capacity of Friedel's salt for the P and L mortars is limited by the amount of Friedel's salt which can be formed, as observed by the apparent plateau for both the experimentally measured and thermodynamically predicted Friedel's salt profiles, when the destabilization of portlandite and ettringite are not taken into account. A comparable plateau in the amount of Friedel's salt is not observed for MK mortars as a result of their very limited chloride ingress depth (about 3 mm). Thermodynamic modelling of the samples with increasing amounts of the NaCl solution has predicted that the portlandite and ettringite are destabilized due to the leaching of calcium resulting in that a somewhat larger amount of Friedel's salt is formed. However, upon advanced leaching the decomposition of Friedel's salt

is predicted which is experimentally confirmed by the observed reduction in the amount of Friedel's salt in the outermost section at the exposed surface.

6 Acknowledgements

The Danish Council for Strategic research is acknowledged the financial support to the LowE-CEM project (No. 11-116724).

7 References

[1] L. Tang, L.-O. Nilsson, P.M. Basheer, Resistance of concrete to chloride ingress: Testing and modelling, CRC Press, 2011.

[2] L. Bertolini, B. Elsener, P. Pedeferri, E. Redaelli, R.B. Polder, Corrosion of steel in concrete: prevention, diagnosis, repair, John Wiley & Sons, 2013.

[3] K. De Weerdt, H. Justnes, M.R. Geiker, Changes in the phase assemblage of concrete exposed to sea water, Cement and Concrete Composites, 47 (2014) 53-63.

[4] R. Loser, B. Lothenbach, A. Leemann, M. Tuchschmid, Chloride resistance of concrete and its binding capacity–Comparison between experimental results and thermodynamic modeling, Cement and Concrete Composites, 32 (2010) 34-42.

[5] I. Galan, F.P. Glasser, Chloride in cement, Advances in Cement Research, 27 (2015) 63-97.

[6] H. Justnes, A review of chloride binding in cementitious systems, Nordic Concrete Research, 21 (1998) 48-63.

[7] Q. Yuan, C. Shi, G. De Schutter, K. Audenaert, D. Deng, Chloride binding of cement-based materials subjected to external chloride environment–a review, Construction and Building Materials, 23 (2009) 1-13.

[8] L. Tang, N. Lars-Olof, Chloride binding capacity and binding isotherms of OPC pastes and mortars, Cement and Concrete Research, 23 (1993) 247-253.

[9] H. Zibara, Binding of external chlorides by cement pastes. (PhD thesis), University of Toronto, Canada., (2001).

[10] K. De Weerdt, D. Orsáková, M. Geiker, The impact of sulphate and magnesium on chloride binding in Portland cement paste, Cement and Concrete Research, 65 (2014) 30-40.

[11] G. Plusquellec, A. Nonat, I. Pochard, Anion uptake by calcium silicate hydrate. 32nd Cement and Concrete Science Conference. Belfast. 17 - 18 Sept. 2012 (paper PRE-4), (2012).

[12] K. De Weerdt, A. Colombo, L. Coppola, H. Justnes, M. Geiker, Impact of the associated cation on chloride binding of Portland cement paste, Cement and Concrete Research, 68 (2015) 196-202.

[13] H. Friedmann, O. Amiri, A. Aït-Mokhtar, Physical modeling of the electrical double layer effects on multispecies ions transport in cement-based materials, Cement and Concrete Research, 38 (2008) 1394-1400.

[14] V. Baroghel-Bouny, X. Wang, M. Thiery, M. Saillio, F. Barberon, Prediction of chloride binding isotherms of cementitious materials by analytical model or numerical inverse analysis, Cement and Concrete Research, 42 (2012) 1207-1224.

[15] D.P. Bentz, E.J. Garboczi, Y. Lu, N. Martys, A.R. Sakulich, W.J. Weiss, Modeling of the influence of transverse cracking on chloride penetration into concrete, Cement and Concrete Composites, 38 (2013) 65-74.

[16] E. L'Hôpital, N. Seigneur, M. Voutilainen, A. Dauzères, Transport properties of cement model system (C3S and C-S-H): Experiments dedicated to implement a new approach of the microstructure / diffusion properties relation in the reactive transport code, in: 4th International Workshop on Mechanisms and Modelling of Waste / Cement Interactions May 22-25, 2016, Murten, Switzerland, 2016.

[17] J. Geng, D. Easterbrook, L.-y. Li, L.-w. Mo, The stability of bound chlorides in cement paste with sulfate attack, Cement and Concrete Research, 68 (2015) 211-222.

[18] J.A. Jain, N. Neithalath, Chloride transport in fly ash and glass powder modified concretes–influence of test methods on microstructure, Cement and Concrete Composites, 32 (2010) 148-156.

[19] R.O. Grishchenko, A.L. Emelina, P.Y. Makarov, Thermodynamic properties and thermal behavior of Friedel's salt, Thermochimica Acta, 570 (2013) 74-79.

[20] U. Birnin-Yauri, F. Glasser, Friedel's salt, Ca2Al(OH)6(Cl,OH)·2H2O: its solid solutions and their role in chloride binding, Cement and Concrete Research, 28 (1998) 1713-1723.

[21] B. Lothenbach, P. Durdzinski, K. De Weerdt, Thermogravimetric analysis. Chater 5 in: A Practical Guide to Microstructural Analysis of Cementitious Materials. Karen Scrivener, Ruben Snellings, and Barbara Lothenbach (Eds.), Taylor & Francis, 2016.

[22] K. De Weerdt, M.R. Geiker, Comparing chloride ingress in Portland cement based binders with slag or fly ash exposed to seawater and deicing salt. (In preparation), (2016).

[23] Z. Dai, Solid-state ^{27}Al and ^{29}Si MAS NMR investigations of white Portland cement - metakaolin blends (PhD thesis), Aarhus University, in, 2015.

[24] Z. Dai, W. Kunther, S. Ferreiro, D. Herfort, J. Skibsted, Investigation of blended systems of supplementary cementitious materials with white Portland cement and limestone (manuscript in preparation), (2016).

[25] H.F.W. Taylor, Modification of the Bogue calculation, Advances in Cement Research, 2 (1989) 73-77.

[26] N. Garg, J. Skibsted, Thermal Activation of a Pure Montmorillonite Clay and its Reactivity in Cementitious Systems, The Journal of Physical Chemistry C, 21 (2014) 11464-11477.

[27] Z. Dai, T.T. Tran, J. Skibsted, Aluminum Incorporation in the C–S–H Phase of White Portland Cement–Metakaolin Blends Studied by ^{27}Al and ^{29}Si MAS NMR Spectroscopy, Journal of the American Ceramic Society, (2014).

[28] M. Geiker, Studies of Portland Cement Hydration by Measurements of Chemical Shrinkage and a Systematic Evaluation of Hydration Curves by Means of the Dispersion Model (thesis), Institute of Mineral Industry, Technical University of Denmark, 1983.

[29] D.A. Kulik, T. Wagner, S.V. Dmytrieva, G. Kosakowski, F.F. Hingerl, K.V. Chudnenko, U.R. Berner, GEM-Selektor geochemical modeling package: revised algorithm and GEMS3K numerical kernel for coupled simulation codes, Computational Geosciences, 17 (2013) 1-24.

[30] T. Wagner, D.A. Kulik, F.F. Hingerl, S.V. Dmytrieva, GEM-Selektor geochemical modeling package: TSolMod library and data interface for multicomponent phase models, The Canadian Mineralogist, 50 (2012) 1173-1195.

[31] B. Lothenbach, T. Matschei, G. Möschner, F.P. Glasser, Thermodynamic modelling of the effect of temperature on the hydration and porosity of Portland cement, Cement and Concrete Research, 38 (2008) 1-18.

[32] M. Balonis, B. Lothenbach, G. Le Saout, F.P. Glasser, Impact of chloride on the mineralogy of hydrated Portland cement systems, Cement and Concrete Research, 40 (2010) 1009-1022.

[33] B. Lothenbach, L. Pelletier-Chaignat, F. Winnefeld, Stability in the system $CaO–Al_2O_3–H_2O$, Cement and Concrete Research, 42 (2012) 1621-1634.

[34] R. Barbarulo, Comportement des matériaux cimentaires: actions des sulfates et de la température (Ph.D. thesis), in, Université Laval Québec, 2002.

[35] H.C. Helgeson, D.H. Kirkham, G.C. Flowers, Theoretical prediction of the thermodynamic behavior of aqueous electrolytes by high pressures and temperatures; IV, Calculation of activity coefficients, osmotic coefficients, and apparent molal and standard and relative partial molal properties to 600 degrees C and 5kb, American journal of science, 281 (1981) 1249-1516.

[36] B.J. Merkel, B. Planer-Friedrich, D. Nordstrom, Groundwater geochemistry, A Practical Guide to Modeling of Natural and Contaminated Aquatic Systems, 2 (2005).

[37] Z. Shi, M.R. Geiker, K. De Weerdt, B. Lothenbach, J. Kaufmann, W. Kunther, S. Ferreiro, D. Herfort, J. Skibsted, Durability of Portland cement blends including calcined clay and limestone: interactions with sulfate, chloride and carbonate ions, in: Calcined Clays for Sustainable Concrete, Springer, 2015, pp. 133-141.

[38] Z. Shi, B. Lothenbach, M.R. Geiker, J. Kaufmann, A. Leemann, S. Ferreiro, J. Skibsted, Experimental studies and thermodynamic modeling of the carbonation of Portland cement, metakaolin and limestone mortars, Cement and Concrete Research, 88 (2016) 60-72.

[39] M. Thomas, R. Hooton, A. Scott, H. Zibara, The effect of supplementary cementitious materials on chloride binding in hardened cement paste, Cement and Concrete Research, 42 (2012) 1-7.

[40] A. Ipavec, T. Vuk, R. Gabrovšek, V. Kaučič, Chloride binding into hydrated blended cements: The influence of limestone and alkalinity, Cement and Concrete Research, 48 (2013) 74-85.

[41] O.M. Jensen, Chloride ingress in cement paste and mortar measured by Electron Probe Micro Analysis, Department of Structural Engineering, Technical University of Denmark, 1999.

[42] C. Andrade, J.M. Diez, A. Alaman, C. Alonso, Mathematical modelling of electrochemical chloride extraction from concrete, Cement and Concrete Research, 25 (1995) 727-740.

[43] U.H. Jakobsen, K. De Weerdt, M.R. Geiker, Elemental zonation in marine concrete, Cement and Concrete Research, 85 (2016) 12-27.

[44] K. De Weerdt, D. Orsáková, A.C.A. Müller, C.K. Larsen, B. Pedersen, M.R. Geiker, Towards the understanding of chloride profiles in marine exposed concrete, impact of leaching and moisture content, Construction and Building Materials, 120 (2016) 418-431.

[45] G. Paul, E. Boccaleri, L. Buzzi, F. Canonico, D. Gastaldi, Friedel's salt formation in sulfoaluminate cements: A combined XRD and ^{27}Al MAS NMR study, Cement and Concrete Research, 67 (2015) 93-102.

[46] Y. Elakneswaran, T. Nawa, K. Kurumisawa, Electrokinetic potential of hydrated cement in relation to adsorption of chlorides, Cement and Concrete Research, 39 (2009) 340-344.

Table 1.

Chemical compositions of the binders (wt.%).

	wPc	MK	SF	LS
SiO_2	21.8	52.8	90.4	3.9
Al_2O_3	3.6	39.5	0.34	0.33
Fe_2O_3	0.236	1.4	0.03	0.14
CaO	66.1	0.22	1.37	53.7
MgO	1.1	0.48	0.93	0.35
K_2O	0.43	1.00	1.87	0.05
Na_2O	0.04	0.05	0.19	0.08
SO_3	3.37	0.06	0.3	0.05
Cl	0.003	0.003	0.13	0.01
LOI (%)	2.6	3.55	3.35	41.8

Table 2.

Compositions of the blends used for the mortars (wt.%).

Mortar labels	Ratio (g/g)	wPc	MK	SF	LS[c]	Si/Al (mol/mol)	Al/Si [a] C-S-H (mol/mol)	S/Si [b] C-S-H (mol/mol)
P	-	100	0	0	0	-	0.067	0.03
L	MK/(MK+LS)=0	68.1	0	0	31.9	-	0.057	0.03
ML	MK/(MK+LS)=0.75	68.1	25.5	0	6.4	1.13	0.092	0.015
M	MK/(MK+LS)=0.94	68.1	31.9	0	0	1.13	0.1	0.015
MSL	(MK+SF)/(MK+SF+LS)=0.75	68.1	15.6	9.88	6.4	2.36	0.095	0.015
MS	(MK+SF)/(MK+SF+LS)=0.94	68.1	19.5	12.4	0	2.36	0.1	0.015

[(a)] Al/Si ratios determined from ^{29}Si MAS NMR for paste samples of the same blends [23].

[(b)] S/Si ratios determined for synthetic C-S-H samples with different Ca/Si ratios [34]. The data are related to the individual samples using the Ca/Si ratios determined for the C-S-H phases in the samples in ref. [23].

[(c)] The amount of LS in this column does not include the 3.1 wt.% of LS in wPc.

Table 3.

Threshold pore size and total porosity for the mortars hydrated for 119 days according to the 1st MIP intrusion curves [37, 38] and apparent chloride diffusion coefficients (D_e) for the mortars exposed to 2.8 M NaCl solution (91 days of water saturated curing plus 35 days of exposure to NaCl solution).

	P	L	ML	M	MSL	MS
Threshold pore radius (nm)	27	32	10	8	11	10
Porosity (v/v, %)	7.6	12.2	7.0	6.8	7.1	7.5
D_e (10^{-12} m^2/s)	7.8	19	0.4	0.9	0.5	0.8

Table 4.

Quantities of Friedel's salt and Portlandite determined by TGA, XRD and GEMs (wt.%) for samples taken at a depth of 1– 2 mm.

Mortar labels	Friedel's salt (wt.%)			Portlandite (wt.%)	
	TGA	XRD	GEMs[a]	TGA	XRD
P	0.8 ± 0.1	0.8 ± 0.2	0.7	2.3 ± 0.3	2.2 ± 0.4
L	0.7 ± 0.1	-	0.7	0.6 ± 0.3	-
ML	1.3 ± 0.2	-	6.9	< 0.1	-
M	0.6 ± 0.1	1.4 ± 0.5[b]	7.2	< 0.1	< 0.2
MSL	1.7 ± 0.2	2.0 ± 0.3	5.1	< 0.1	0.5 ± 0.2
MS	1.2 ± 0.2	1.7 ± 0.3	5.9	< 0.1	< 0.2

(a) The predicted amount of Friedel's salt is derived as the quantity corresponding to the depletion of monocarbonate.

(b) This sample does not contain anatase and thus, no quantitative Rietveld analysis can be performed. However, considering the intensity and width of the primary reflection from Friedel's salt in this sample compared to the other three samples allows estimation of 1.4 ± 0.5 wt.% Friedel's in this sample.

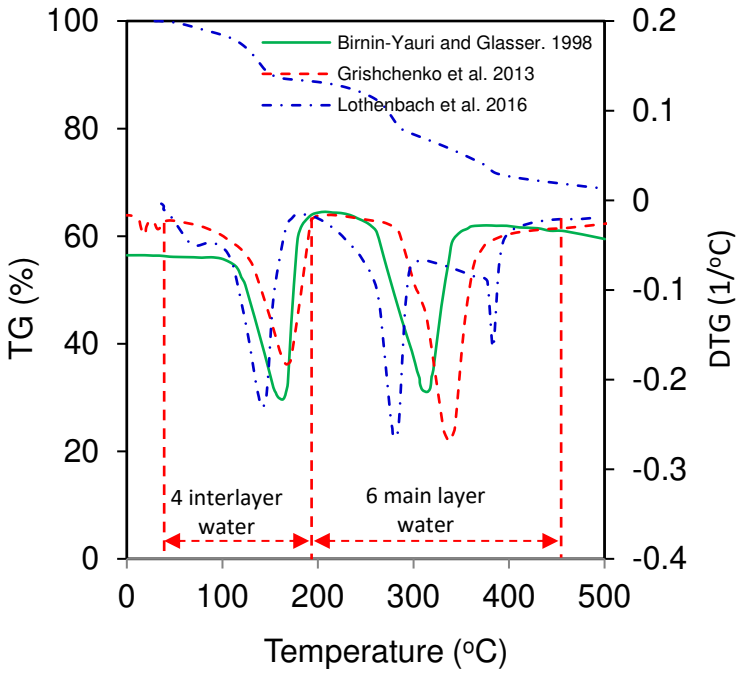

Fig. 1. Characterization of synthesized samples of Friedel's salt by TGA [19-21].

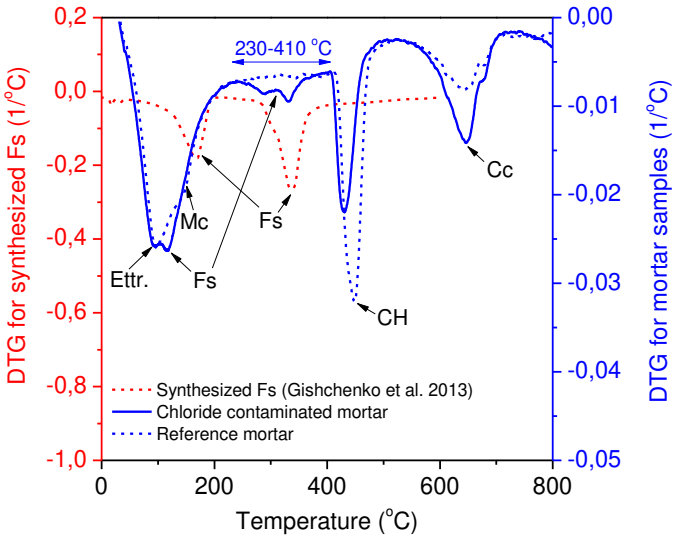

Fig. 2. Quantification of Friedel's salt in a chloride exposed mortar cylinder (P) using TGA. The chloride-containing sample was obtained at mortar depth 1~2 mm, the reference sample containing no chlroide was obtained from the same mortar at a depth of 8~12 mm. Ettr. : ettringite, Mc: monocarbonate, Fs: Friedel's salt, CH: portlandite, Cc: $CaCO_3$.

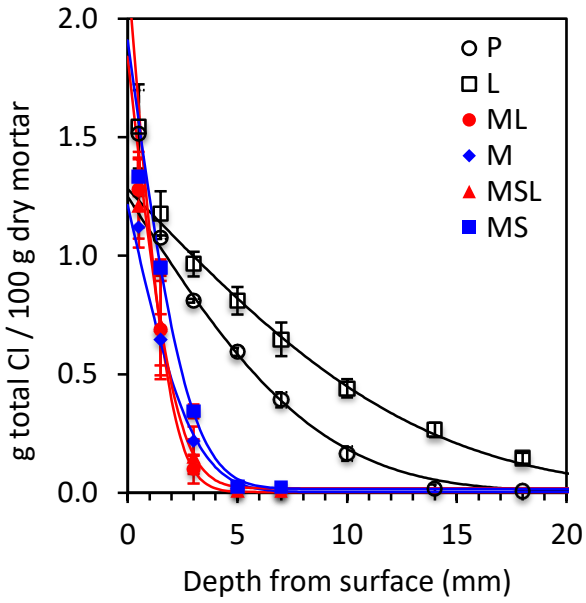

Fig. 3. Total chloride profiles for the studied mortars. The powdered mortar samples obtained at different depths of mortars were dried in an oven at 105 ^{o}C for 24 hours prior to the total chloride profile analysis.

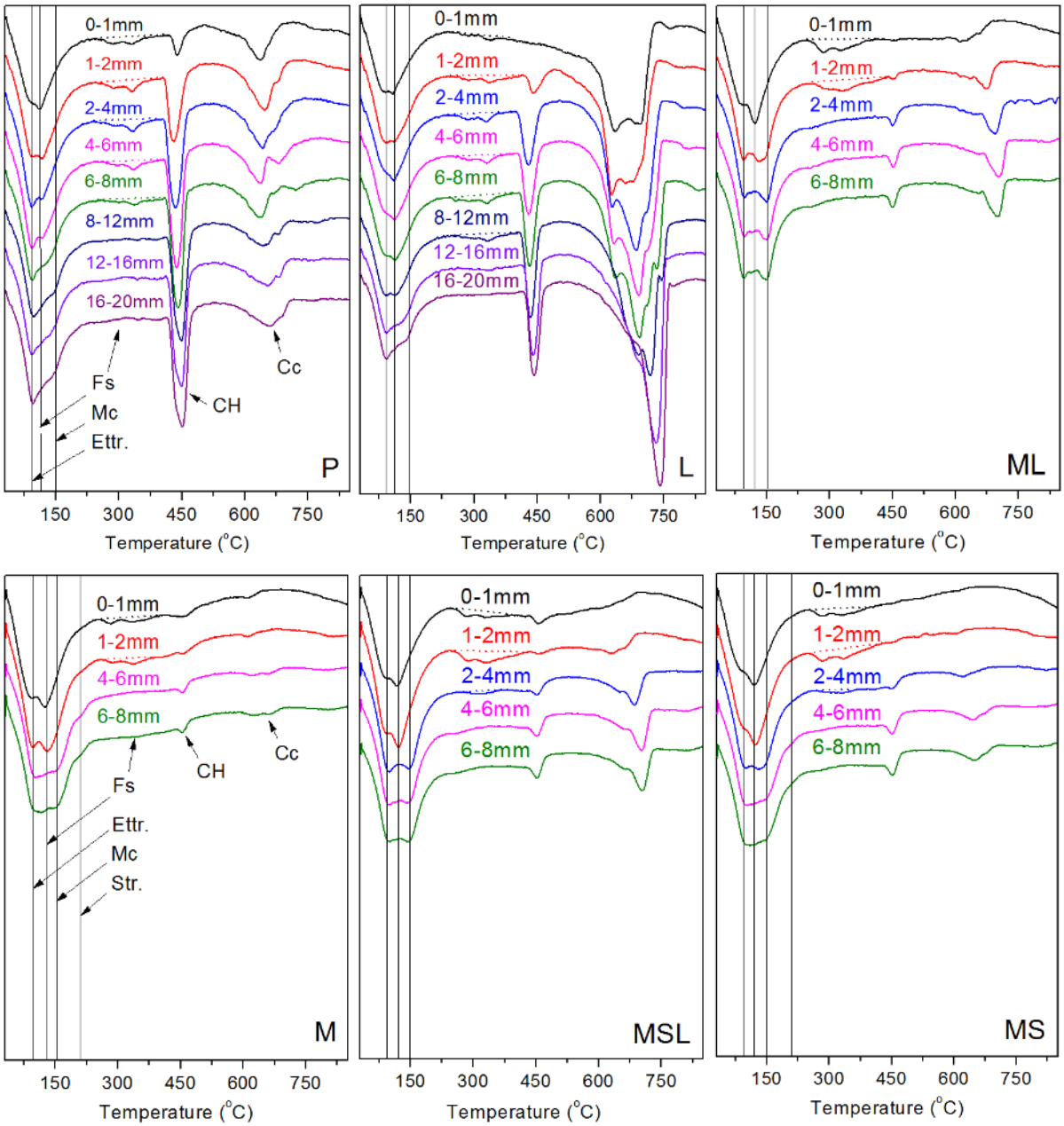

Fig. 4. DTG curves of the same powdered mortar samples as used for total chloride profile analysis (Fig. 3). Ettr. : ettringite, Mc: monocarbonate, Fs: Friedel's salt, Str. : strätlingite, CH: portlandite, Cc: $CaCO_3$. Peak assignments according to [21].

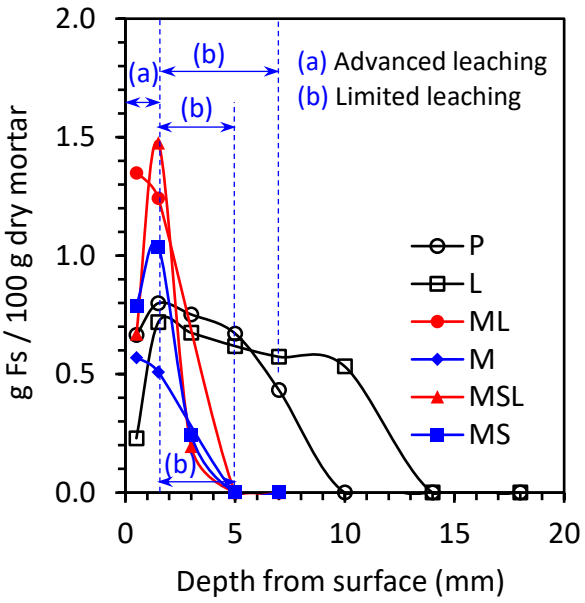

Fig.5. Friedel's salt (Fs) profiles measured by TGA for the studied mortars. The amounts of Friedel's salt are obtained from Fig. 4 using the method described in section 2.4.

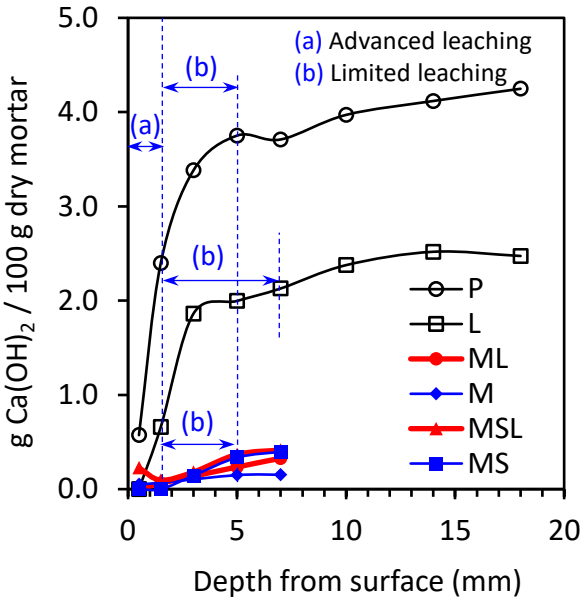

Fig.6. Portlandite (CH) profiles measured by TGA for the studied mortars. The amounts of CH are obtained from Fig. 4 using the method described in section 2.4.

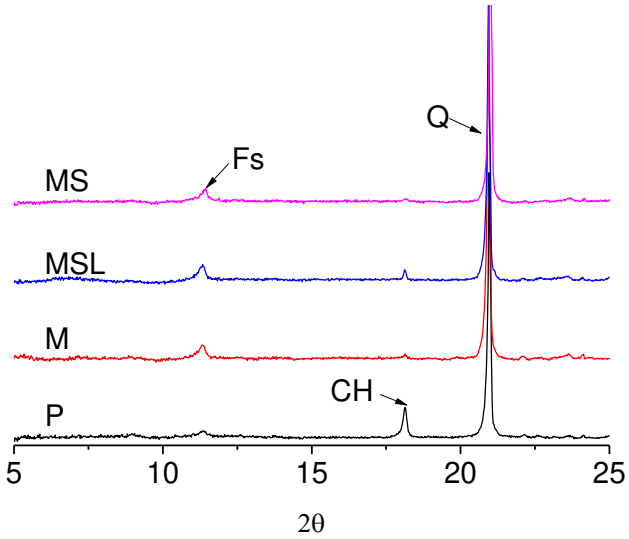

Fig. 7. Friedel's salt in the P, M, MS and MSL mortars measured by XRD. The samples are obtained from the mortar at 1 - 2 mm depths. (Fs: Friedel's salt, CH: portlandite, Q: quartz).

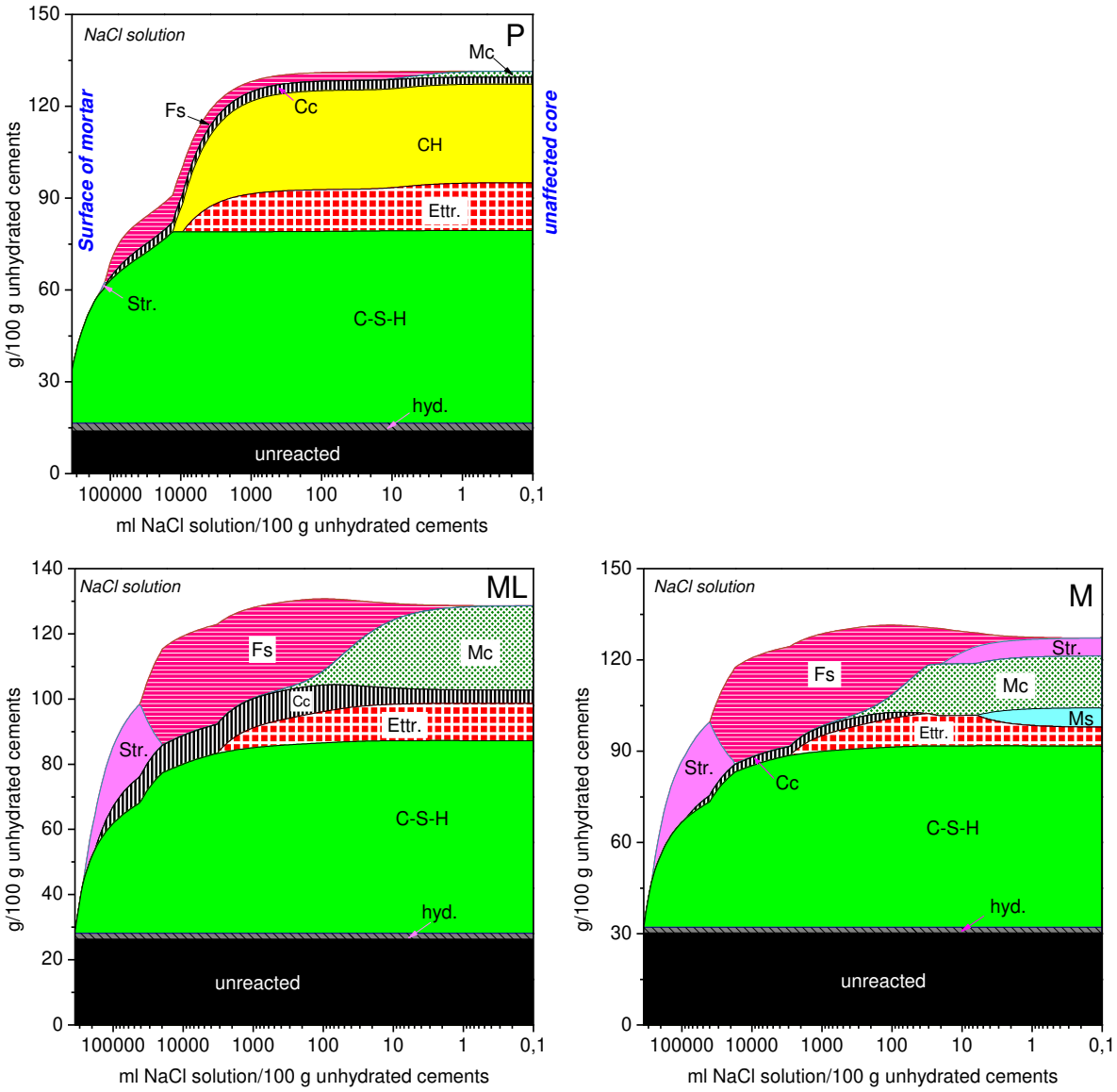

Fig. 8. Changes in phase assemblages predicted by thermodynamic modelling for paste samples of the P, ML and M blends in contact with different quantities of the 2.8 M NaCl solution. A variation of the amount of NaCl solution allows simulation of the ingress of chloride ions, assuming that the surface of the mortar is in contact with a large amount of NaCl solution while the center of the mortar is in contact with no or very little NaCl solution. The right-hand side of the graphs is referred to the inner core of the mortar and the left-hand side to the surface of the mortar. The phase assemblages for the L, MSL and M blends are similar to the P, ML and M mortars, respectively. Hyd.: hydrotalcite; C-S-H: calcium-silicate-hydrate; CH: portlandite; Cc: calcium carbonate; Ettr.: ettringite; Mc: monocarbonate; Str.: strätlingite; Fs: Friedel's salt.

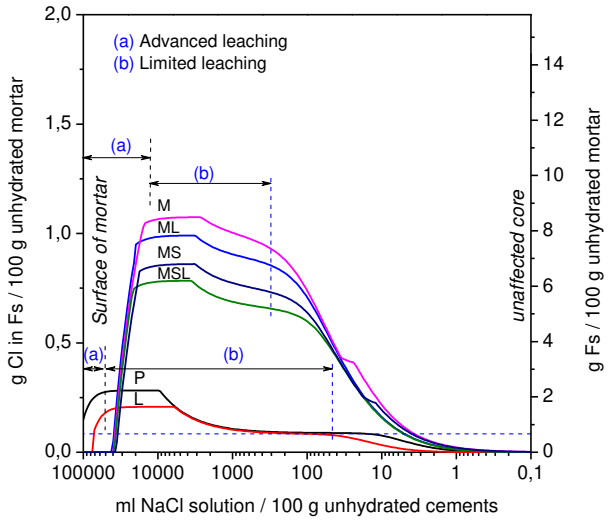

Fig. 9. Calculated profiles for chloride bound in Friedel's salt (Fs), left-hand scale, and Friedel's salt profiles (right-hand scale) obtained by thermodynamic modelling for the different mortar samples exposed to 2.8 M NaCl solutions. Both measures for Friedel's salt have been divided by a factor of 4 to account for the binder/sand ratio of 3 for the mortars, *i.e.*, for a direct comparison with the experimental results from TGA and XRD (Fig. 5 and Table 4).

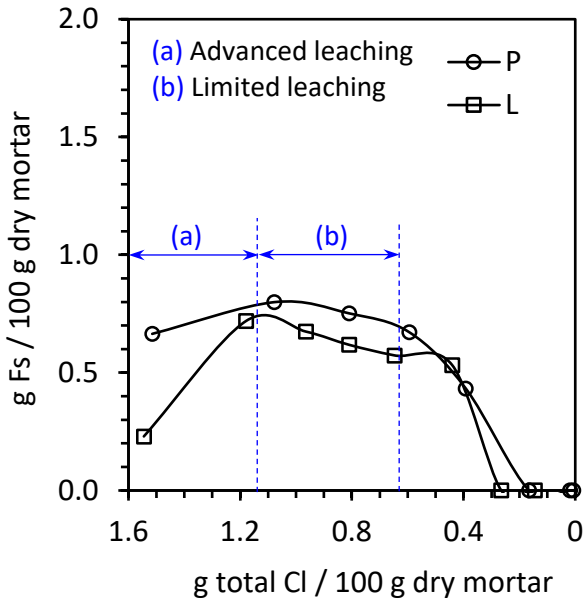

Fig. 10. Correlation of the total chloride content (by tritration) and the measured amount of Friedel's salt (by TGA) formed in the studied mortars.

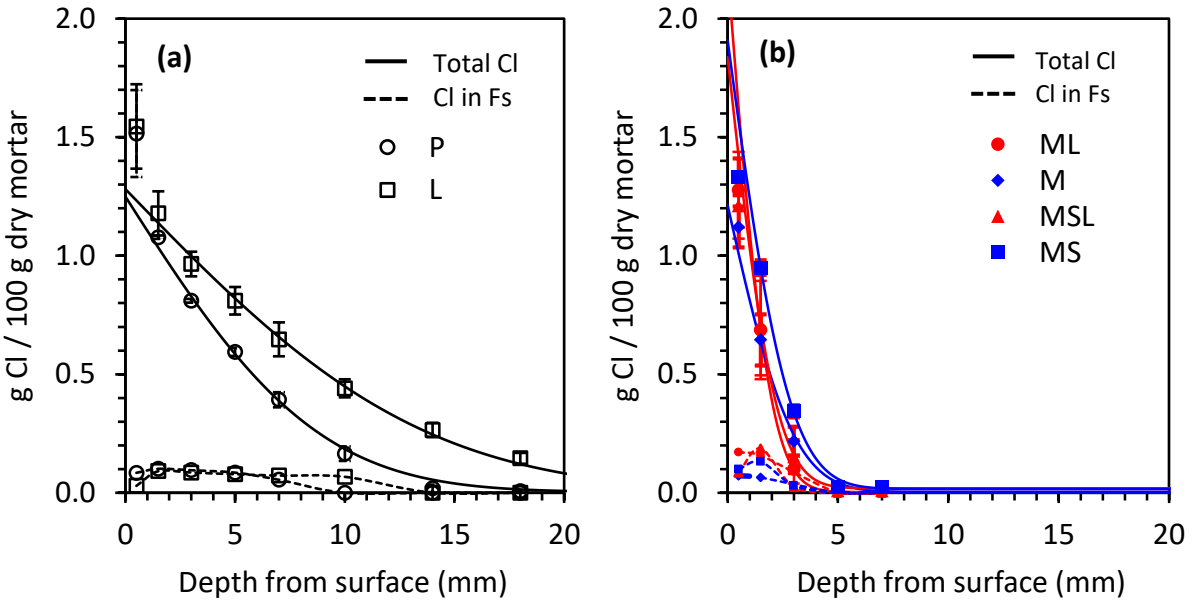

Fig. 11. Comparison of the total chloride profiles and the bound chloride profiles in Friedel's salt measured by TGA for (a) the reference mortars (P and L) and (b) the four metakaolin-containing mortars (ML, M, MSL and MS).